ORIENTAL JOURNAL OF CHEMISTRY
An International Open Access, Peer Reviewed Research Journal
www.orientjchem.org
ISSN: 0970-020 X
CODEN: OJCHEG
2025, Vol. 41, No.(1):
Pg. 111-119

Supercapacitor Performance and Characterization of La Doped V_2O_5 Nanoparticles

NAGASUNDAR S[1]*, ANU KALIANI A[1], SUBIN S[2] and SAKUNTHALA AYYASAMY[2]

[1]*Department of Physics, Kongunadu Arts and Science College, Coimbatore, Tamil Nadu, 641-029, India.
[2]Division of Physical Sciences, Karunya Institute of Technology and Sciences, Coimbatore, Tamil Nadu, 641-114, India.
*Corresponding author E-mail: nagasundar542@gmail.com, anuplasmakasc@gmail.com

http://dx.doi.org/10.13005/ojc/410112

(Received: December 27, 2024; Accepted: January 31, 2025)

ABSTRACT

Supercapacitors as energy storage devices and their unique position within the spectrum of energy storage technologies. Lanthanum-doped vanadium oxide nanoparticles were synthesized using the co-precipitation method. The Prepared samples were under gone various characterization such as X-Ray Diffraction, UV-Vis spectroscopy, Photoluminescence, FT-IR, and SEM. X-Ray Diffraction (XRD) studies confirms the orthorhombic crystal structure of La doped V_2O_5 nanoparticles. UV-Vis spectroscopy estimates as slight increase in band gap (E_g) from 3.28 eV (pure V_2O_5) to 3.47 eV (La doped V_2O_5). The Photoluminescence emission inters the increase in oxygen vacancies in La doped V_2O_5. From the results of FTIR spectra, it was observed that the peaks are shifted from lower to higher wavenumbers (right side) and lies between 555 to 680nm. The size of the Pure V_2O_5 particles is from 41-54nm where the size of the La doped V_2O_5 Nanoparticle. It is 41-101nm estimated by Sem analysis. The elemental analysis of pure V_2O_5 nanoparticles predicted the chemical compositions of V and C are about 92.83% and 7.17% and in 5% La doped V_2O_5 nanoparticles the chemical compositions of V, La and C are about to be about 77.19%, 4.50% and 18.31% respectively. CV studies shows that 5% of La doped V_2O_5 nanoparticles have reached the highest discharge capability of 172.96 F/cm^2 in 5mV with a good cyclic reversibility. The GCD analysis determined that the specific capacitance of 5% La-doped V_2O_5 nanoparticles was approximately 119.96 F/g at a discharge current of 0.5 A/g.

Keyword: Vanadium pentoxide (V_2O_5), Lanthanum oxide (La) doping, Cyclic voltammetry (CV), GCD and EIS (Impendence analysis).

INTRODUCTION

Transition metal oxides such as Vanadium Pentoxide (V_2O_5), is a potential electrode material for high-efficiency supercapacitors due to their exceptional electrochemical properties. V_2O_5 exhibits attractive characteristics but further enhancements are sought to maximize its energy storage capabilities[1-3]. It is observed that doping strategies have gained significant attention and hence the dopant Lanthanum (La) has been chosen. La-based compounds such as La $(NO_3)_3$ are recognized for their high specific capacitance with high power density, they are well-suited for high-potential electrode materials[4]. However, traditional fabrication methods and the use of binders often involve

complex procedures which can hinder Recently, there has been a growing interest in binder-free electrodes which eliminate the need for additional materials that can compromise performance. This method simplifies fabrication and enhances the electrochemical efficiency of supercapacitors. By focusing on binder-free electrode fabrication and optimization of charge-discharge behaviour and enhancement of overall the energy storage capacity and power sustainability of supercapacitor devices was studied[5,6]. The insights gained from this work have significant implications for the development of advanced energy storage solutions for diverse applications, such as portable electronics, electric vehicles, and renewable energy systems.

EXPERIMENTAL METHODS

Synthesis of La doped V_2O_5 nanoparticles

Pure V_2O_5 nanoparticles was synthesised by using the co-precipitation method. Initially, 5–10 drops of HCl were mixed for 1 mol solution of V_2O_5 and 10–15 min using magnetic stirrer. A precipitation was obtained and it was rinsed twice using DI water and then ethanol. The rinsed yellowish-white precipitation was dried for 24 h in room temperature to remove the moisture content. It was annealed at 600 for 3 hours. The synthesised Pure V_2O_5 nanoparticles are collected from the filter paper. The collected samples were then grinding with a mortar for 10 min for further study. The same procedure is followed for La doped V_2O_5 at different wt% such as 3%, 5%, and 7%.

Preparation of pure V_2O_5 and La doped V_2O_5 electrodes

For the preparation of functional electrode, the pure Vanadium pentoxide nanoparticles, NMP, and polyvinylidene fluoride (PVDF) are combined in a mass ratio of 16:3:1 to create a uniform mixture. mixture for the electrochemical experiment. Subsequently, this substance is applied onto a nickel foam substrate to create a functional electrode. The reference auxiliary electrode consisted of a platinum wire and nickel foam (NF) sheet which was used as the working electrode on to which 7 mg V_2O_5 nano powder was coated. The same procedure was repeated for 5% La doped V_2O_5 nanoparticles also. The performance of V_2O_5 electrodes is assessed at electrochemical workstation by cyclic voltammetry (CV) analysis.

Characterization Techniques

Energy Dispersive Spectroscopy (EDS)-equipped Field Emission Scanning Electron Microscopy (FE-SEM, JSM 6500F, JEOL, Tokyo, Japan) was used to properties the surface of the produced V_2O_5 and La-doped V_2O_5 nanoparticle. Using an X-ray diffractometer (Cu Kα rays), the crystal structures and phases of every sample were examined. FTIR spectroscopy was used to study the particle composition and chemical state. The UV-Vis was used to conduct the NIR and UV-Vis spectroscopy investigation. The materials of the nanoparticle's microstructure were imaged using a sophisticated technique (FE-SEM). CV, GCD, and EIS (Impendence) methodologies were used to conduct the electrochemical investigations.

RESULT AND DISSCUSION

XRD Analysis

Figure 1 presents the XRD analysis of both pure V_2O_5 and La-doped V_2O_5 nanoparticles. The findings from the XRD studies indicates that the major peaks shifted to higher angles due to the addition of dopants at varying concentrations. Measurements were taken from 10° to 80° at a scanning rate of 0.4° min^{-1}. Notably, La doped V_2O_5 nanoparticles showed a more significant shift at a doping concentration of 5% wt. The most prominent diffraction peaks (010) exhibited a slight right shift toward higher angles compared to pure V_2O_5 nanoparticles, confirming an orthorhombic structure that aligns with the standard reference (JCPDS card No. 00-001-0359) for V_2O_5. This shift in the XRD positions of doped vanadium suggests successful incorporation of La into the host structure at the V^{5+} sites, which may be reason for an increase in crystallite size (D). The dominant peak of the nanoparticles is noted at an angle 20.23° (2θ, corresponding to the Miller indices (0 1 0).

$$D = \frac{0.89\lambda}{\beta\ COS\theta}$$

In the Scherrer equation, D represents the average crystallite size, β represents the peak width at half maximum, θ represents the diffraction angle, and λ represents the wavelength of Cu Kα radiation. With increasing doping concentration, the average crystallite size increases. This growth is likely caused by particle aggregation. Specifically, the crystallite size increases from 71.25 nm for pure V_2O_5 to 90.68 nm for the 5% La-doped sample. This change correlates with a decrease in the full width at half maximum and an increase in the intensity of the (2 0 0) plane. The similarity in ionic radii between La^{3+} (0.65 Å) and V^{5+} (0.54 Å), from previous studies reported in the literature[7].

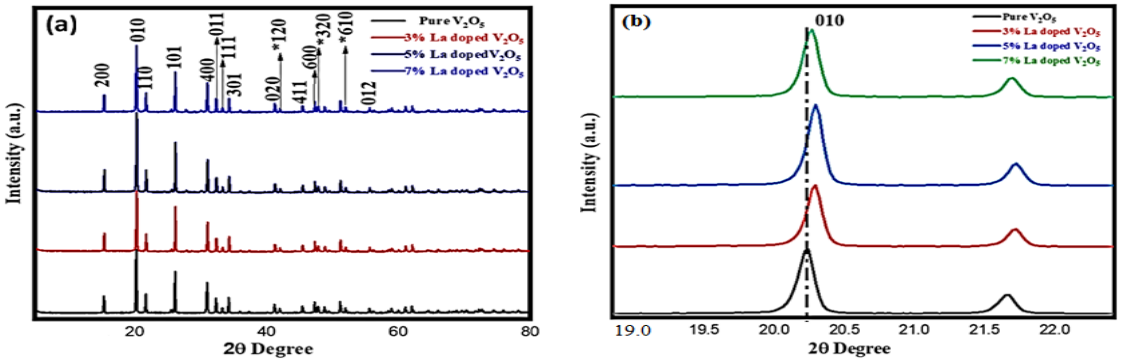

Fig. 1(a). XRD graph for Pure V_2O_5 and La doped V_2O_5 nanoparticles and (b) Right shifting of the prominent peaks in the samples

FT-IR Spectra analysis

Figure 2, This study showed the FTIR spectra of pure V_2O_5 and La-doped V_2O_5 annealed at 600°C in the range 532-840 cm^{-1}. The absorption band at 432 cm^{-1} is attributed to the V-O vibrations which may activate V_2O_5 surface[8,9].

The FTIR spectra peaks of pure V_2O_5 and La doped V_2O_5 nanoparticles exhibit a slight shift in peak towards higher wavenumbers (right side)[10]. This shift indicates improved La efficiency. The shift range is between 555 and 680 cm^{-1}. Absorption bands are interface of La doped V_2O_5 confirming the presence of distinct compounds formed during V-O-V absorption above 600°C.

FTIR spectra of activated La doped V_2O_5 revealed that the observed bands between 532-617 cm^{-1} may be attributed to absorption. The peak originated from 555 cm^{-1} is due to species cross-linked at the edges of activated V_2O_5 nanoparticles, whereas the peak at 680 cm^{-1} arises from species bound to active V-O-V[5]. The stretching vibration of the La surface on activated La-doped V_2O_5 causes the broad band spanning 725 to 840 cm^{-1}

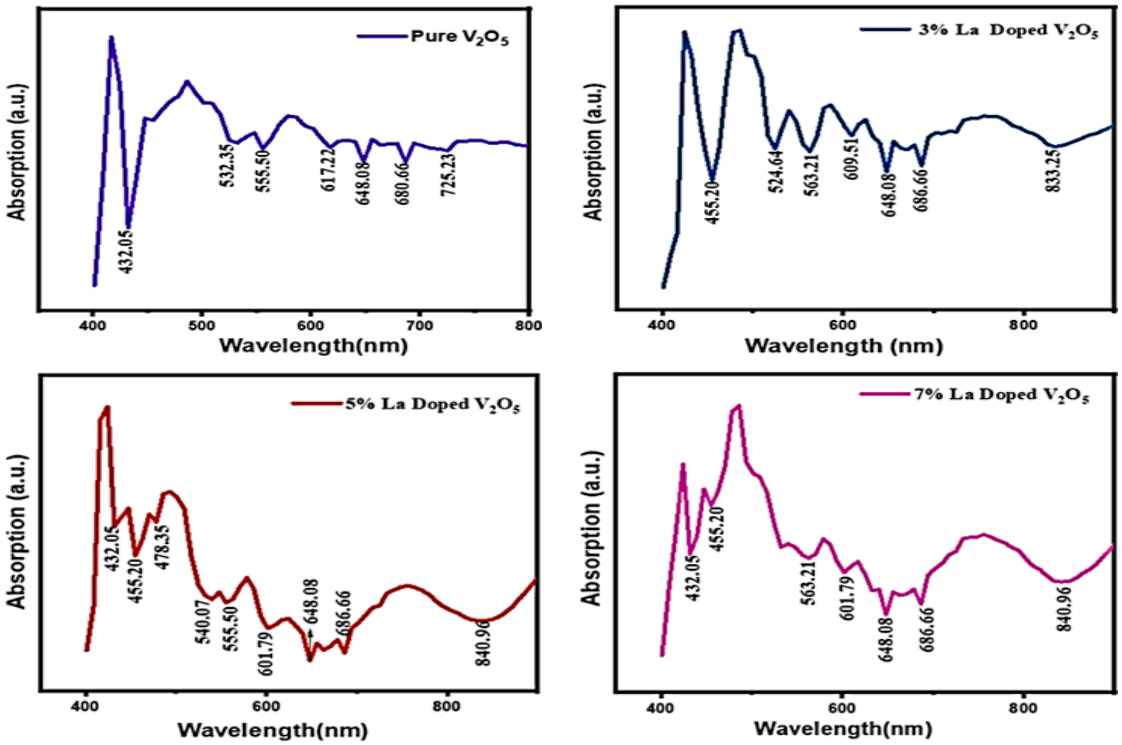

Fig. 2. FT-IR Spectrum analysis for Pure V_2O_5 and La doped V_2O_5 nanoparticles

The peaks disappeared FT-IR studied indicates the removal of loose absorption species during the calcination. It was conformed with XRD analysis.

UV-Visible Analysis

Strong absorption bands are observed in the range of 420 to 440 nm which is corresponding to the charge transfer band of V_2O_5[11]. Fig. 3(a) shows the UV-Visible absorption spectrum of La doped V_2O_5 sample.

The absorption band observed between 600-800 nm range, indicates that the d-d transition of the vanadyl group. It evidences the presence of V^{4+} ions, in the spectrum. The absence of V^{4+} ions suggests that most vanadium species are in the oxidized V^{5+} form, although the minor presence of V^{4+} ions cannot be ruled out[12].

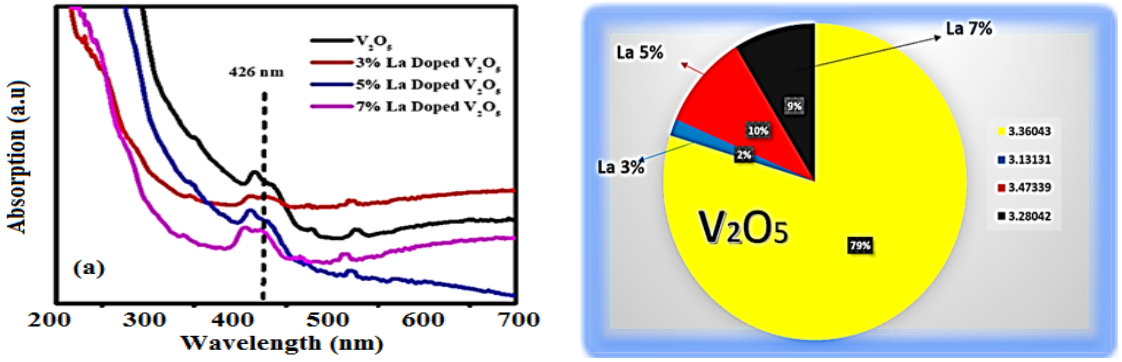

Fig. 3(a). UV-Visible spectroscopy analysis pure V_2O_5 and La doped V_2O_5 nanoparticles and absorption of band gap energy level

The absorption spectrum from the Fig. 3(a) it can be observed that shows a slight shift towards longer wavelengths. This may be due to the incorporation of La doped V_2O_5 lattice significantly and it reduces the band gap. Fig. 3(a) Band gap energies for pure V_2O_5 and La-doped V_2O_5 samples (3%, 5%, and 7% La) are compared in the pie chart, band gap energy calculated using the Tauc plot equation for the experimentally observed energy levels.

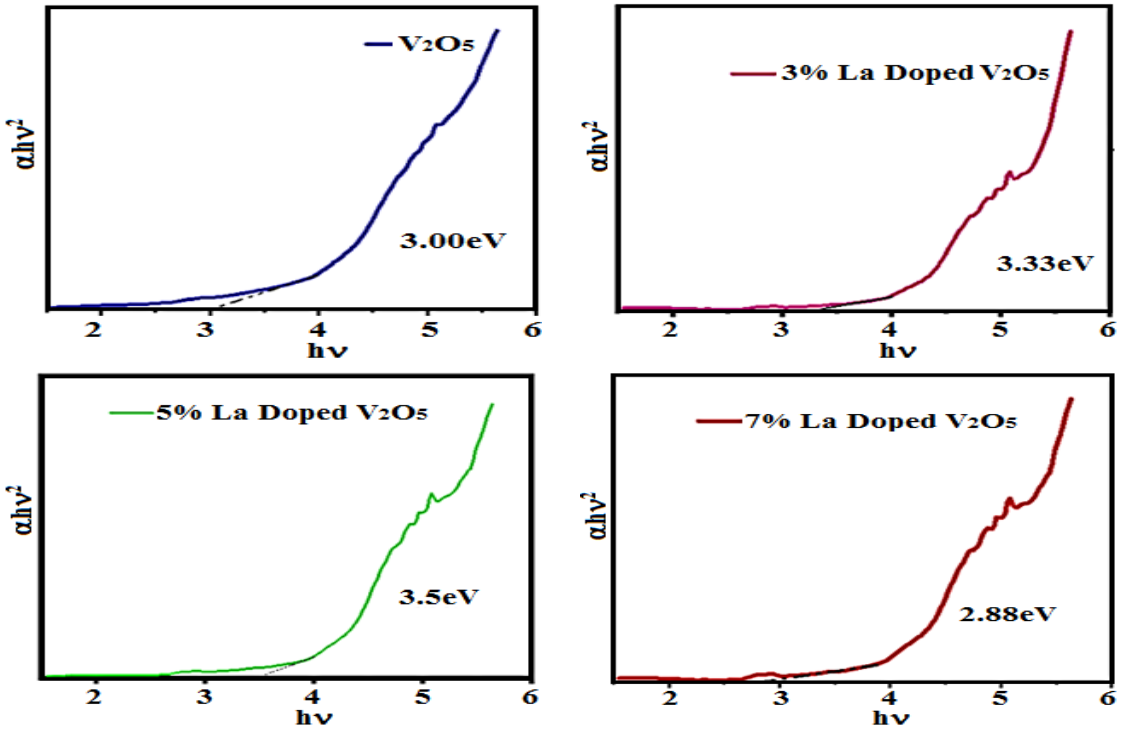

Fig. 3(b). Band gap energy of pure V_2O_5 and La doped V_2O_5 nanoparticles

To determine the band gap energy (Eg) of the samples, determined using the Tauc plot method, is presented below.

$$Eg = \frac{hc}{\lambda}$$

Where relates band gap energy (Eg), Planck's constant (h), the speed of light (c), and the wavelength of maximum absorption (λ).[13]

The plot in Fig. 3(b) illustrates the Tauc plot analysis, where the rising area represents the calculated band gap values for the samples. The obtained Eg values (3.28-3.47 eV) are consistent and the average bandgap energy of La doped V_2O_5 nanoparticles is 3.31 eV.

Photoluminescence (PL) Analysis

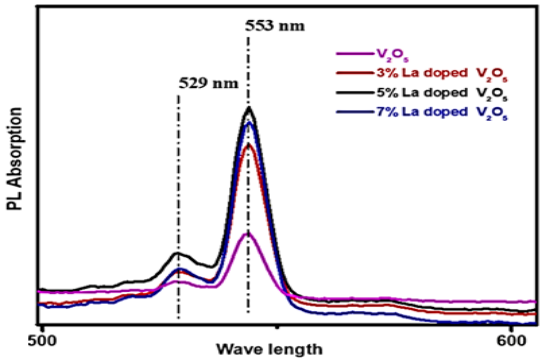

Fig. 4. Emission for PL spectra for pure V_2O_5 nanoparticles and La doped V_2O_5 nanoparticles

Figure 4 presents the photoluminescence (PL) spectra of V_2O_5 nanoparticles. V_2O_5 nanoparticle precursors exhibit two emission bands: one in the UV-region, which scientists attribute to exciton-exciton collision processes, and another in the visible region, which scientists attribute to electron-hole recombination within the band gap.

A broad peak appears around 529nm and 553nm in the visible range. Annealing at 600°C enhances this visible PL emission, likely due to single-ionized oxygen vacancies (VO^+) at 529nm. Doping V_2O_5 often leads to oxygen loss. This increase in PL emission intensity is strongly associated with a significant rise in band gap energy observed in La doped V_2O_5 nanoparticles at 5% of La doping.

SEM Analysis

The FESEM image of pure V_2O_5 and various percentage of La doped V_2O_5 (3%,5% and 7% by Wt. percentage) are shown in Fig. 5(a-d). From the Fig. it is observed that pure V_2O_5 nanoparticles exhibit nanoflake structure with rough and uniform grain boundary whereas La doped V_2O_5 are formed with uneven surfaces and rough edges.

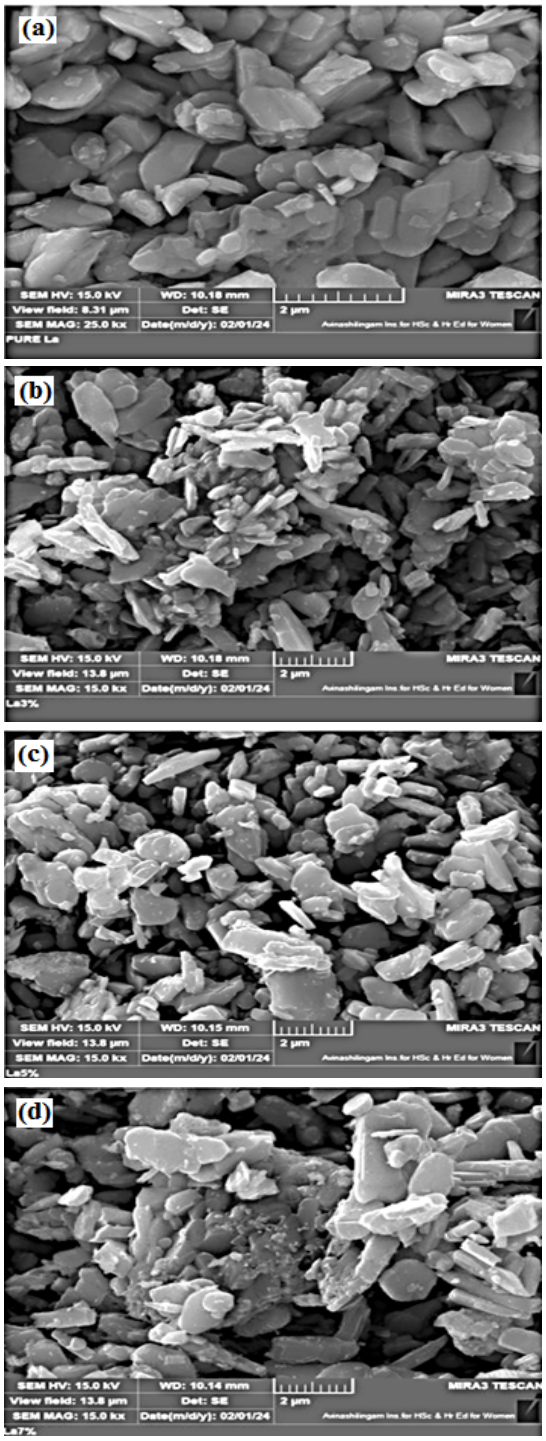

Fig. 5. FESEM image of Pure V_2O_5 and various concentration of La doped V_2O_5 nanoparticles

From the SEM image, average particles size of V_2O_5 nanoparticles is observed between 41-54nm and for La doped V_2O_5 the average particle size ranges from 46-101nm. Morphology studies of pure V_2O_5 and La doped V_2O_5 nanoparticles reveal that 5% of La doped V_2O_5 nanoparticles shows nanoflakes structure. which significantly enhances supercapacitor property when compared to the other samples (pure V_2O_5, 3% La and 7% La doped V_2O_5 nanoparticles).

It is reported in literature[15] that nanoflakes structure (Fig. 5c) play an important role for enhancing supercapacitor property.

Energy Dispersive Analysis X-ray (EDAX) Studies

Elemental nanoparticles analysis of pure V_2O_5 and various percentage of La doped V_2O_5 nanoparticles were carried out using EDAX.

The EDAX spectra of pure V_2O_5 and La-doped V_2O_5 nanoparticle samples are displayed in Fig. 6. In the pure V_2O_5 nanoparticle samples, the chemical compositions of V and C are found to be 77.19% and 18.31% Wt, respectively. For the La-doped V_2O_5 nanoparticle samples, the chemical composition of La is found to be 4.50% Wt.

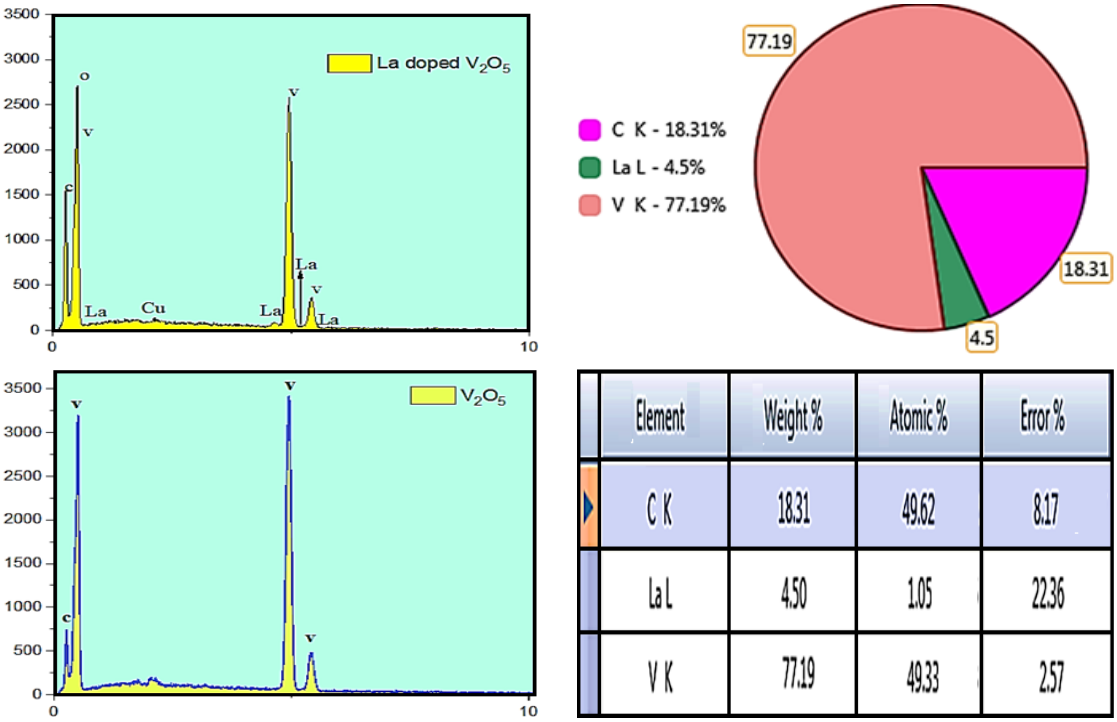

Element	Weight %	Atomic %	Error %
C K	18.31	49.62	8.17
La L	4.50	1.05	22.36
V K	77.19	49.33	2.57

Fig. 6. EDAX spectra of pureV_2O_5 and La doped V_2O_5 nanoparticles

Electrochemical studies

Cyclic voltametric (CV)

Electrochemical performance was investigated Fig. 7(a) and (b) shows cyclic voltametric (CV) graphs for pure and 5% La-doped V_2O_5 nanoparticle electrodes, recorded using a three-electrode system (platinum counter electrode, Ag/AgCl reference electrode, V_2O_5 working electrode, 1M KOH electrolyte) within a potential window of -0.7 to 0.6 V at scan rates from 5 to 100 mV/s. All samples showed oxidation and reduction peaks in the CV plots, demonstrating capacitive behaviour and indicating the pseudo-capacitive nature of the material[16]. The specific capacitance of the material was calculated from the CV curve using the following formula,

$$Specific\ Capacitance = \frac{A}{M \times K \times V}$$

Where A is Area under the curve, M is Mass of the active material, K is Scan rate, and V is Potential window.

Specific capacitance values arrived from CV curves were 191.72 and 172.96 F/cm² for pure and 5% of La doped V_2O_5 nanoparticles respectively. Notably, V_2O_5 nanoparticles doped with 5% of La exhibit higher capacitance. CV curves for 5% of La

doped V_2O_5 nanoparticles at different scan rates were taken and from the result It was observed that the quasi-rectangular shape of the CV curves is affected by the scan rate, with specific capacitance increasing as the scan rate increases[17]. This is due to the fact that a higher scan rate enhances the utilization of the electrode's effective area, leading to an increased specific capacity.

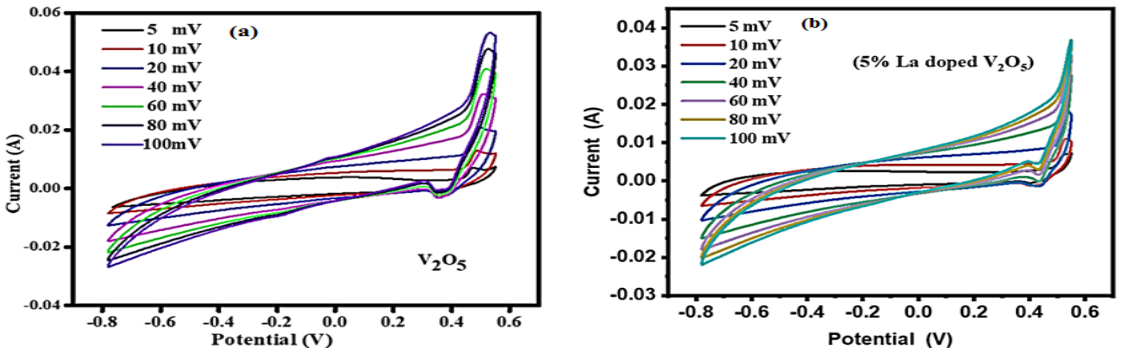

Fig. 7(a) and (b) CV Graph of Pure V_2O_5 and 5% of La doped V_2O_5 nanoparticles

X-ray diffraction (XRD) and CV result indicate that the specific capacitance of the nanoparticles is primarily influenced by two factors. one is the intensity of the (200) planes of the stable V_2O_5 layered structure and the another is the sample's surface roughness which may be determined by the doping concentration[18]. Nanoparticles synthesized with 5% La doping exhibited significant surface roughness with predominant (010) planes showing comparatively high specific capacitance thom other La doped V_2O_5 nanoparticles.

Galvanostatic charge-discharge (GCD)

Galvanostatic charge-discharge (GCD) was employed to investigate the charge storage performance of the material and to understand the sustainability of the La doped V_2O_5 nanoparticles for supercapacitor electrodes.

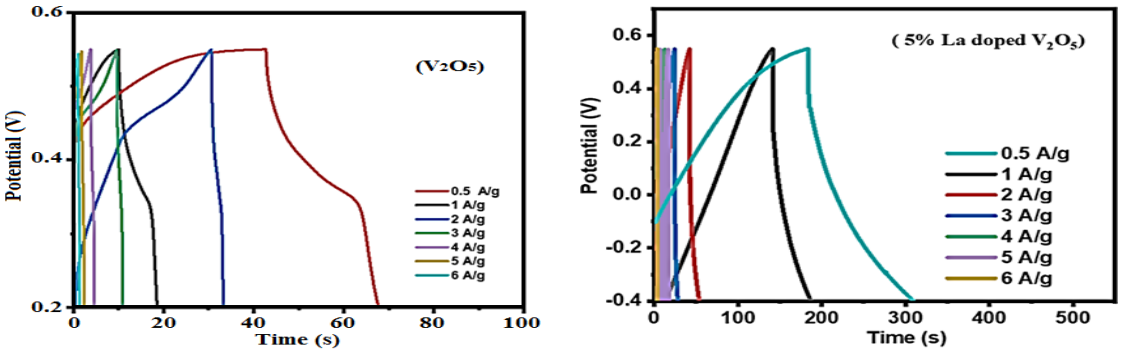

Fig. 8. GCD curves are Pure V_2O_5 and 5 % of La doped V_2O_5 nanoparticles

GCD measurements (0.5-6 A/g) were performed using a three-electrode system (same potential window as CV studies). The specific capacitance was calculated from the GCD graph. Fig. 8 shows the results.

$$Cp = \frac{I \times \Delta t}{M \times \Delta V}$$

Where I is the current, Δt is the discharge time, M is the mass, and ΔV is the potential window difference.

La-doped V_2O_5 nanoparticles exhibited the highest specific capacitance in the GCD studies, reaching 119.96 F/g at 0.5 A/g. The nanoparticles retained a specific capacitance of 11.27 F/g even at 6 A/g.

Impendence analysis

Figure 9 shows electrochemical behaviour of La doped V_2O_5 nanoparticles on electrode using electrochemical impedance spectroscopy (EIS). This may be utilized to determine the internal resistance (RS) and charge transfer resistance (RCT).

EIS measurements were performed within a frequency range of 0.1 to 10 kHz, with an

AC amplitude of 10 mV and an equilibrium time of 1 second. In the EIS results, no semicircle was observed in the high-frequency range due to the low charge transfer resistance.

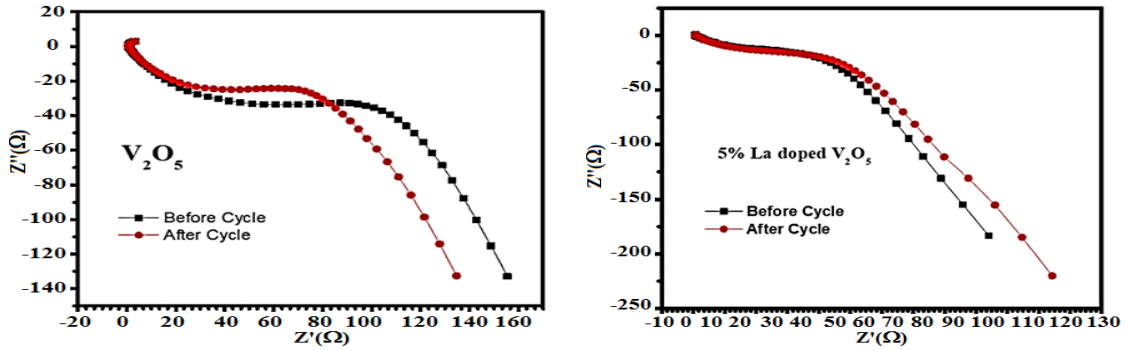

Fig. 9. Impendence analysisGraph of Pure V_2O_5 and 5% of La doped V_2O_5 nanoparticles current density

Cyclic voltammetry (CV) profiles at different scan rates, along with cyclic stability and resistive behaviour assessments indicate the electrode's potential for supercapacitor applications showing promising charge storage performance[19].

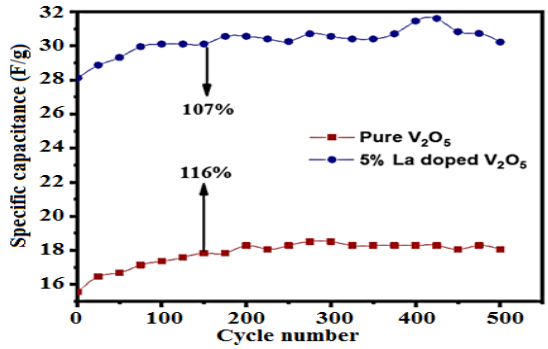

Fig. 10. Cyclic stability of pure V_2O_5 and 5% La doped V_2O_5 nanoparticles

The reduced gaps between nanoparticles enhance the electrode's charge storage and conversion efficiency. Fig. 10 shows the results of a 500-cycle cyclic stability test conducted on pure V_2O_5 and La-doped V_2O_5 nanoparticles. Pure V_2O_5 exhibits a cyclic stability of 116%, while La-doped V_2O_5 shows 107% at 2A/g. This indicates that the cyclic stability of La-doped V_2O_5 nanoparticles is lower than that of pure V_2O_5 for supercapacitor applications.

CONCLUSION

This study discusses the structural, optical, and electrochemical properties of lanthanum-doped vanadium pentoxide (V_2O_5) nanoparticles. XRD analysis of La doped V_2O_5 NPs shows an orthorhombic structure. FT-IR spectroscopy reveals the presence of alky halide groups contributing to the absorption peak in the visible region. UV-Vis spectroscopy showed an optical band gap energy in the range 3.28-3.47 eV. This aligns with the reported values of La-doped V_2O_5. Photoluminescence (PL) emission spectra showed broad peaks in the visible region with enhanced intensity when the NPs were annealed at 600°C for 3 hours. This could be attributed to an increase in single-ionized oxygen vacancies (VO^+). Notably, 5% La doped V_2O_5 nanoparticles exhibited a significant rise in oxygen vacancies which correlates the observed nanoflakes structure revealed by FE-SEM analysis. Electrochemical characterization using Cyclic Voltammetry (CV), Galvanostatic Charge-Discharge (GCD), and Electrochemical Impedance Spectroscopy (EIS) demonstrated enhanced supercapacitor performance for La-doped V_2O_5 nanoparticles compared to pure V_2O_5. Notably, 5% La-doped V_2O_5 nanoparticles achieved the highest specific capacitance of 119.96 F/g at a current density of 0.5 A/g. These results underscore the potential of La-doped V_2O_5 nanoparticles as a promising electrode material for high-performance supercapacitor applications.

ACKNOWLEDGMENT

This research did not receive any specific grant from funding agencies in the public, commercial, or not-for-profit sectors.

Conflict of interest

The author declare that we have no conflict of interest.

REFERENCES

1. Farahmandjou M. Chemical Synthesis of Vanadium Oxide (V_2O_5) Nanoparticles Prepared by Sodium Metavanadate., *J Nanomed Res.*, **2017,** *18*;*5*(1).
2. Zimmermann R.; Claessen R.; Reinert F.; Steiner P.; Hüfner S. Strong hybridization in vanadium oxides: evidence from photoemission and absorption spectroscopy [Internet]. Vol. *10*, J. Phys.: Condens. Matter. **1998**. Available from: http://iopscience.iop.org/0953-8984/10/25/018
3. Müller O.; Goering E.; Urbach JP.; Weber T.; Paulin H.; Klemm M.; Metal-insulator transition of VO_2. A XANES investigation of the O K edge of VO_2., *Journal De Physique* IV : JP., **1997**, *7*(2 Part 1).
4. Ma Z.; Rui K.; Zhang Y.; Li D.; Wang Q.; Zhang Q., Nitrogen Boosts Defective Vanadium Oxide from Semiconducting to Metallic Merit., *Small.*, **2019,** *29*;15(22).
5. Bibi Jaffri S.; Shahzad Ahmad K.; Abrahams I.; Ibrahim AA. Semiconductor V_2O_5-ZnO nano-rods driven efficient photovoltaic and electrochemical performance in multitudinous applications., *Materials Science and Engineering*: B., **2023,** *1*, 298.
6. Liao H.; Zhong W.; Li C.; Han J.; Sun X.; Xia X., An intrinsically self-healing and anti-freezing molecular chains induced polyacrylamide-based hydrogel electrolytes for zinc manganese dioxide batteries., *Journal of Energy Chemistry.*, **2024,** *1*(89), 565–78.
7. Mahato S.; Puigdollers J. Tempera. dependent current-voltage characteristics of Au/n-Si Schottky barrier diodes and the effect of transition metal oxides as an interface layer., *Physica B Condens Matter.*, **2018,** *1*(530), 327–35.
8. Kerli S.; Alver Ü.; Eskalen H.; UruşS.; Soşuksu AK. Structural and Morphological Properties of Boron Doped V_2O_5 Thin Films: Highly Efficient Photocatalytic Degradation of Methyl Blue., *Russian Journal of Applied Chemistry.*, **2019,** *1*;*92*(2), 304–9.
9. John Chelliah CRA.; Swaminathan R. Improved optical absorption, enhanced morphological and electrochemical properties of pulsed laser deposited binary zinc and vanadium oxide thin films., *Journal of Materials Science: Materials in Electronics.*, **2020,** *1*;*31*(10), 7348–58.
10. Ceccarelli M.; Barthel FP.; Malta TM.; Sabedot TS.; Salama SR.; Murray BA., Molecular Profiling Reveals Biologically Discrete Subsets and Pathways of Progression in Diffuse Glioma., *Cell.*, **2016,** *28*, *164*(3), 550–63.
11. Balasubramani V.; Chandrasekaran J.; Marnadu R.; Vivek P.; Maruthamuthu S.; Rajesh S. Impact of Annealing Temperature on Spin Coated V_2O_5 Thin Films as Interfacial Layer in Cu/V_2O_5/n-Si Structured Schottky Barrier Diodes., *J Inorg Organomet Polym Mater.*, **2019,** *1;29*(5), 1533–47.
12. Harish Senthil P.; Chandrasekaran J.; Marnadu R.; Balraju P.; Mahendarn C. Influence of high dielectric HfO_2 thin films on the electrical properties of Al/HfO_2/n-Si (MIS) structured Schottky barrier diodes., *Physica B Condens Matter.*, **2020,** *1*, 594.
13. Akl AA. Effect of solution molarity on the characteristics of vanadium pentoxide thin film., *Appl Surf Sci.*, **2006,***15;252*(24), 8745–50.
14. Chen D.; Cheng Y.; Zhou N.; Chen P.; Wang Y.; Li K., Photocatalytic degradation of organic pollutants using TiO_2-based photocatalysts: a review **2020**.
15. Mai L.; An Q.; Wei Q.; Fei J.; Zhang P.; Xu X., Nanoflakes-assembled three-dimensional hollow-porous V_2O_5 as lithium storage cathodes with high-rate capacity., *Small*, **2014** *13;10*(15), 3032–7.
16. Beke S. A review of the growth of V_2O_5 films from **1885** to **2010**. Vol. 519., *Thin Solid Films.*, **2011**, 1761–71.
17. Ben Elkamel I.; Hamdaoui N.; Mezni A.; Ajjel R.; Beji L. Synthesis and characterization of Cu doped ZnO nanoparticles for stable and fast response UV photodetector at low noise current., *Journal of Materials Science: Materials in Electronics.*, **2019,** *30;30*(10), 9444–54.
18. Mahato S.; Biswas D.; Gerling LG.; Voz C.; Puigdollers J. Analysis of temperature dependent current-voltage and capacitance-voltage characteristics of an Au/V_2O_5/n-Si Schottky diode., *AIP Adv.*, **2017,** *1;7*(8).
19. Salanne M.; Rotenberg B.; Naoi K.; Kaneko K.; Taberna PL.; Grey CP., Efficient storage mechanisms for building better supercapacitors. Vol. 1, Nature Energy. Nature Publishing Group; **2016**.